JOURNAL OF GEOPHYSICAL RESEARCH, VOL. 115, F01009, doi:10.1029/2009JF001444, 2010



# A review of snow and ice albedo and the development of a new physically based broadband albedo parameterization

Alex S. Gardner[1] and Martin J. Sharp[1]

Received 8 July 2009; revised 15 September 2009; accepted 2 October 2009; published 5 March 2010.

[1] We present a computationally simple, theoretically based parameterization for the broadband albedo of snow and ice that can accurately reproduce the theoretical broadband albedo under a wide range of snow, ice, and atmospheric conditions. Depending on its application, this parameterization requires between one and five input parameters. These parameters are specific surface area of snow/ice, concentration of light-absorbing carbon, solar zenith angle, cloud optical thickness, and snow depth. The parameterization is derived by fitting equations to albedo estimates generated with a 16-stream plane-parallel, discrete ordinates radiative transfer model of snow and ice that is coupled to a similar model of the atmosphere. Output from this model is also used to establish the physical determinants of the spectral albedo of snow and ice and evaluate the characteristics of spectral irradiance over snow-covered surfaces. Broadband albedo estimates determined from the radiative transfer model are compared with results from a selection of previously proposed parameterizations. Compared to these parameterizations, the newly proposed parameterization produces accurate results for a much wider range of snow, ice, and atmospheric conditions.

**Citation:** Gardner, A. S., and M. J. Sharp (2010), A review of snow and ice albedo and the development of a new physically based broadband albedo parameterization, *J. Geophys. Res.*, *115*, F01009, doi:10.1029/2009JF001444.

## 1. Introduction

[2] Under most atmospheric conditions, absorption of shortwave radiation is the largest energy source for melting snow and ice [*Male and Granger*, 1981; *Paterson*, 2000]. The amount of shortwave radiation absorbed is dependent on both the incident radiation and the surface albedo, both of which are highly variable in space and time [*Stroeve et al.*, 1997; *Klok et al.*, 2003]. It is therefore critical to incorporate the temporal variability of snow and ice albedo in numerical models of the surface energy balance. This can be done either by specifying the albedo on the basis of continuous observations, or by computing it with a physical model or empirically based parameterization. Direct surface measurements of snow and ice albedo are sparse, discontinuous, and often contain large errors if the instrumentation is not continuously monitored [*van den Broeke et al.*, 2004]. Satellite derived albedos offer more spatially continuous data sets but are limited to times of clear sky overpasses and may contain significant sources of error, especially over complex terrain [*Stroeve et al.*, 1997; *Klok et al.*, 2003]. For these reasons, numerical models of snow and ice albedo are often incorporated into surface energy balance and climate models.

[3] Sophisticated radiation transfer models do a very good job at producing snow and ice albedo estimates that closely match observations [*Grenfell et al.*, 1994; *Aoki et al.*, 2000; *Painter et al.*, 2007], but they are computationally demanding and require many inputs that are not routinely available. Thus, surface energy balance and climate models typically employ computationally simple albedo parameterizations that require minimal inputs in one or more spectral bands. Despite the strong influence of snow and ice albedo on climate, surface energy balance, and melt rates [*Cess et al.*, 1991; *Klok and Oerlemans*, 2004], there is little consensus on which albedo parameterizations are most appropriate for large-scale modeling.

[4] The theoretical determinants of the spectral albedo ($a_\lambda$) of snow and ice are well established [*Warren and Wiscombe*, 1980; *Wiscombe and Warren*, 1980; *Warren*, 1982; *Mullen and Warren*, 1988; *Askebjer et al.*, 1997; *Warren et al.*, 2002; *Ackermann et al.*, 2006; *Warren and Brandt*, 2008], but there have been few attempts to derive theoretically based, computationally simple broadband (spectrally integrated) albedo parameterizations that are easily implemented in surface energy balance and climate models [*Marshall*, 1989; *Brun et al.*, 1992]. Thus, most such models employ empirical parameterizations [e.g., *Brock et al.*, 2000; *Pedersen and Winther*, 2005] developed from observational data sets. These parameterizations are practical in that they provide a reasonable approximation of snow and ice albedo while requiring minimal knowledge of the physical characteristics of the snow, ice and atmosphere. They are, however, somewhat limited in their applicability as they are based on statistical fits to albedo measurements that are representative of the characteristics of the snow, ice, and atmosphere for specific time periods and locations.

[1]Department of Earth and Atmospheric Sciences, University of Alberta, Edmonton, Alberta, Canada.


0148-0227/10/2009JF001444$09.00

[5] This motivates the development of a computationally simple, theoretically based parameterization for snow and ice albedo that can accurately reproduce theoretical broadband albedos under a wide range of snow, ice, and atmospheric conditions. The parameterization is derived by fitting equations to broadband albedo estimates generated with a 16-stream plane-parallel, discrete ordinates radiative transfer model of snow and ice that is coupled to a similar model of the atmosphere. This allows for simulation of multiple reflections between the surface and atmosphere that alter the spectral distribution of solar irradiance. This is important because the modification of the spectral distribution of solar irradiance by clouds can significantly modify the broadband albedo of snow and ice [*Grenfell and Maykut*, 1977; *Carroll and Fitch*, 1981; *Grenfell and Perovich*, 1984; *Jonsell et al.*, 2003; *Grenfell and Perovich*, 2008].

[6] As the goal of this study is to develop a theoretically based parameterization, we start by reviewing what is known about radiative transfer in snow and ice and discussing the physical determinants governing its albedo. This review supplements earlier works [*Grenfell and Maykut*, 1977; *Warren and Wiscombe*, 1980; *Wiscombe and Warren*, 1980; *Grenfell et al.*, 1981; *Warren*, 1982; *Mullen and Warren*, 1988; *Grenfell et al.*, 1994] with a more complete discussion of the solar irradiance and the inclusion of many new references.

[7] This paper is divided into 6 sections: Section 2 describes how the single scattering properties (optical properties of the individual constituents) of snow and ice were determined and discusses the formulation of the coupled snow and ice–atmosphere radiative transfer model. Section 3 uses output from this model to establish the physical determinants of the spectral albedo of snow and ice and evaluates the characteristics of spectral irradiance over snow-covered surfaces. Section 4 compares broadband albedos determined from the model with results from a selection of previously proposed parameterizations, and suggests a new parameterization of broadband albedo. The final two sections discuss this new parameterization and summarize the main conclusions of the paper.

## 2. Radiative Transfer Modeling of Snow, Ice, and the Atmosphere

### 2.1. Single Scattering

[8] To define the optical characteristics of snow and ice we must first determine the single scattering properties of its individual constituents (e.g., ice grains, air bubbles, and impurities). As long as the individual particles are sufficiently separate that they act as independent scatterers, the scattering properties of a single element can be characterized by three dimensionless optical characteristics; the absorption efficiency $Q_{abs}$, scattering efficiency $Q_{sca}$, and asymmetry factor $g$ (mean cosine of the scattering angle). For ease of calculation, particles are often assumed to scatter as spheres. If one knows the radius $r$ of the sphere and the complex refractive index of the medium ($m_\lambda = n_\lambda + ik_\lambda$), then the dimensionless optical characteristics can be determined using Mie theory [*Bohren and Huffman*, 1998].

[9] In models which resolve the absorption and scattering of shortwave radiation by snow and ice, the optical geometries of ice grains can be well described by a collection of spheres that have the same specific surface area ($\hat{S}$, surface area per unit mass) as the snow grains they describe [*Hansen and Travis*, 1974; *Warren*, 1982; *Grenfell et al.*, 1994]. The area-weighted mean radius of these optically equivalent grains is referred to as the effective radius, $r_e$, and is directly related to specific surface area as

$$r_e = \frac{3}{\rho_i \hat{S}}$$

where $\rho_i$ is the density of ice (910 kg m$^{-3}$). Optical properties relevant to energy balance studies modeled using this definition of effective radius agree well with observations and exact model results for a wide range of grain sizes, wavelengths, optical depths and several different crystal shapes [*Grenfell and Warren*, 1999; *Neshyba et al.*, 2003; *Grenfell et al.*, 2005]. This allows for significant model simplification as complex snow grain geometries and orientations can be modeled as optically equivalent spheres.

[10] In a pure ice sample which contains only air bubbles, all photon absorption events will occur within the ice and all scattering will occur at the ice-bubble boundaries. Scattering efficiencies and asymmetry parameters are, therefore, purely a function of the effective bubble size and can be calculated using Mie theory in the same way as for snow grains but with the absorption set equal to zero ($m_\lambda = n_\lambda$,) [*Mullen and Warren*, 1988]. Absorption, on the other hand, is solely a function of the amount of ice per unit volume and the absorbance of ice.

[11] In this analysis $Q_{abs}$, $Q_{sca}$, and $g$ for spherical ice grains, air bubbles and light-absorbing carbon were determined for 381 wavelengths from 0.2 to 4.0 $\mu$m using the algorithms developed by *Mätzler* [2002]. The complex refractive index for ice was taken from *Warren and Brandt* [2008]. The optical properties of light-absorbing carbon, commonly referred to as "black carbon" or "soot," were determined using the spectrally uniform complex index of refraction suggested by *Bond and Bergstrom* [2006] ($m$ = 1.95 + 0.79$i$). There are large uncertainties regarding the absorptive properties of light-absorbing carbon in snow and ice. This is because typical ratios of internally (particles residing within the ice grains) to externally (carbon particles located outside the ice grains) mixed carbon particles in terrestrial snow are not well known, and carbon particle densities, sizes, and refractive indices vary with production sources and residence times in the atmosphere [*Bond and Bergstrom*, 2006]. For this study, carbon particles are assumed to be externally mixed, have an effective radius of 0.1 $\mu$m [*Horvath*, 1993; *Hansen and Nazarenko*, 2004], and a mean density of 1.8 g cm$^{-3}$ [*Bond and Bergstrom*, 2006]. The mass absorption coefficient (MAC) of the prescribed light absorbing carbon varies across the solar spectrum. The MAC decreases rapidly from its largest value of 6.8 m$^2$ g$^{-1}$ at 0.4 $\mu$m to 3.6 m$^2$ g$^{-1}$ at 1 $\mu$m and continues to decreases to 0.7 m$^2$ g$^{-1}$ at 4 $\mu$m.

[12] For the sake of computational simplicity, we chose not to model dust within snow and ice. This choice is justifiable because (1) carbon is ~200 times more absorbent by mass than crustal dust at visible wavelengths, (2) dust has been shown to have significantly less impact on snow

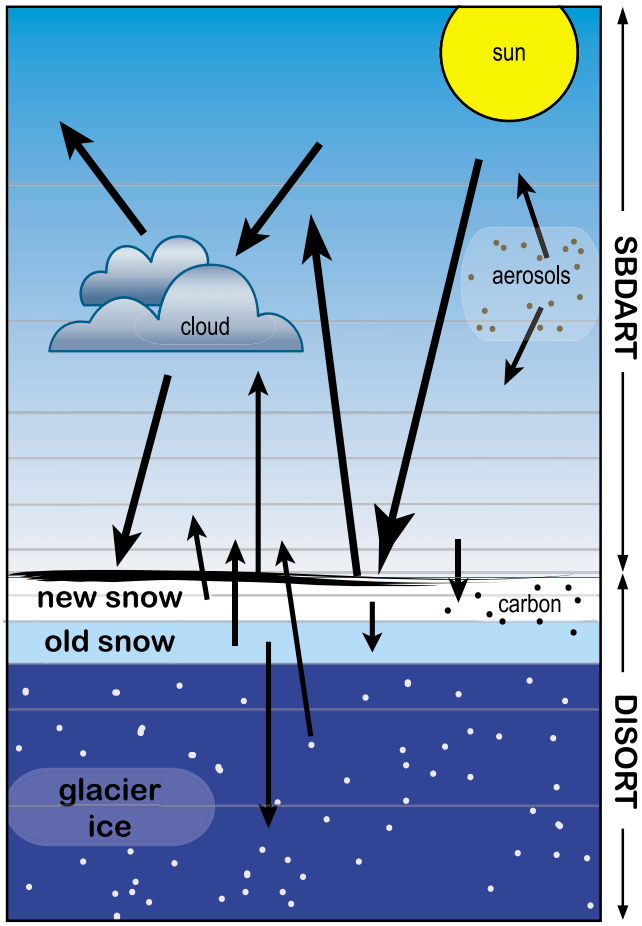


**Figure 1.** Schematic diagram showing the coupled snow and ice–atmosphere radiative transfer model.

albedo than light-absorbing carbon in remote areas devoid of local dust sources, and (3) the effects on broadband albedo of dust loading in snow and ice should be similar to those of optically equivalent concentrations of light-absorbing carbon [*Warren and Wiscombe*, 1980; *Warren*, 1984; *Warren and Clarke*, 1990]. Effects of other snow impurities, such as organic debris and algae, that can reduce albedo [*Grenfell*, 1991] are not examined in this study.

[13] All Mie calculations (for ice, soot and air) were averaged over 1000 effective radii with a Gaussian distribution ($u = r_e$, $\sigma = 0.15r_e$). This minimized ripple effects in calculated Mie values which are not observed in natural media that contain a range of particle sizes [*Bohren and Huffman*, 1998, pp. 296–305].

### 2.2. Multiple Scattering

[14] The single scattering properties were used to determine snow and ice layer optical depths and single scattering albedos. Scattering phase functions were determined using the Henyey–Greenstein approximation, which has been shown to work well for the calculation of snow spectral albedo [*Aoki et al.*, 2000]. These derived variables were then used to define varying snow and ice conditions in a 16-stream plane-parallel discrete ordinates radiative transfer model (DISORT) [*Stamnes et al.*, 1988].

[15] For accurate estimation of spectrally integrated broadband albedo, it was necessary to couple the snow and ice model with the Santa Barbara DISORT Atmospheric Radiative Transfer model (SBDART 2.4) [*Ricchiazzi et al.*, 1998]. This allowed for simulation of multiple reflections between the surface and the atmosphere that can have a significant influence on the amount, spectral distribution, and fractions of direct and diffuse solar radiation incident at the surface, all of which influence the broadband albedo of snow [*Grenfell and Maykut*, 1977; *Carroll and Fitch*, 1981; *Grenfell and Perovich*, 1984; *Grenfell and Perovich*, 2008]. Within SBDART, we assigned a sub-Arctic summer standard atmospheric profile [*McClatchey et al.*, 1972] and a surface elevation of sea level. A schematic diagram illustrating key components of the coupled snow and ice–atmosphere model is provided in Figure 1.

[16] Where radiative transfer modeling was performed for cloudy conditions, clouds were assigned the characteristics of Arctic summertime lower-level stratus clouds. This is the predominant cloud type in the Arctic during summer months (when snow and ice melt occurs) and accounts for approximately 85–90% of all summer cloud cover observed over the Arctic Ocean [*Serreze and Barry*, 2005, p. 48]. All clouds were assumed to be evenly distributed between the elevations of 1000 to 2500 m asl and were assigned an effective droplet radius of 7.5 $\mu$m, a value typical of Arctic summertime low-level stratus [*Curry et al.*, 1996]. The uncertainty in the effective radius of cloud droplets introduces little error in estimates of cloud radiative properties [*Fitzpatrick et al.*, 2004].

## 3. Determinants of the Albedo of Snow and Ice

[17] The amount of energy absorbed by a medium at a specific wavelength is dependent on its spectral albedo $\alpha_\lambda$ which is defined as the ratio of the reflected $F_\lambda^\uparrow$ to incident $F_\lambda^\downarrow$ flux as referenced to a specified surface. The spectral albedo of snow and ice is dependent on the optical properties of its individual constituents, the location and frequency of scattering and absorption events, and radiation's angle of incidence. When shortwave radiative fluxes are discussed in terms of one or more spectral bands, the amount of energy absorbed by the medium is determined using spectrally integrated albedos ($\alpha$). Spectrally integrated albedos are dependent on both the spectral albedo of the medium and the spectral distribution of the incident irradiance within each spectral band. To understand the determinants of the spectrally integrated albedo of snow and ice, it is therefore necessary to examine the determinants of their spectral albedos and the characteristics of the solar spectral irradiance.

### 3.1. Location and Frequency of Scattering and Absorption Events

[18] The spectral albedo $\alpha_\lambda$ of snow and ice varies greatly across the solar spectrum (Figure 2), with $\alpha_\lambda \approx 1$ in the near-ultraviolet and visible regions ($\lambda = 0.3$–$0.7$ $\mu$m), and $\alpha_\lambda < 0.4$ in the shortwave infrared region ($\lambda = 1.5$–$5.0$ $\mu$m). Outside the near-ultraviolet wavelengths, the albedo of pure snow is highly sensitive to effective grain size (Figure 2). This can best be understood by considering radiative transfer as a statistical process. Neglecting internal scatter-

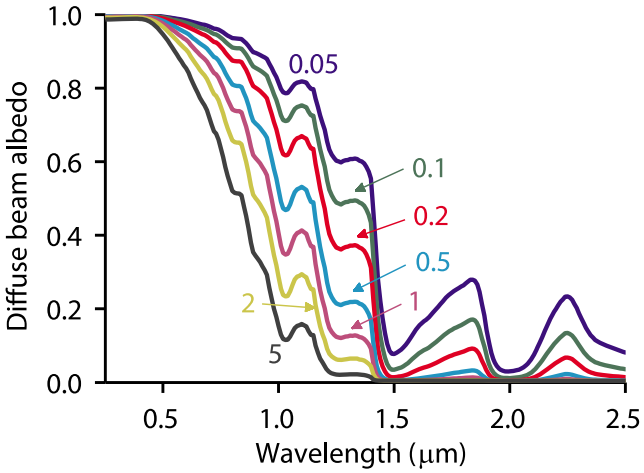


**Figure 2.** Semi-infinite diffuse beam pure snow albedo as a function of the effective grain radius $r_e$ (mm).

ing (scattering not at snow grain boundaries) and absorption by interstitial air, a photon has a chance of being scattered at the air-ice interface and a chance of being absorbed while passing through the ice. An increase in the average radius of the ice grains effectively increases the length of the photon's travel path through the ice and decreases the number of opportunities for the photon to scatter out of the snowpack. This increases the probability of the photon being absorbed and, in more general terms, reduces the surface albedo.

[19] Small amounts of strongly absorbent impurities, such as soot, dust and volcanic ash, lower snow albedo in the spectral region where absorption by ice is weakest ($\lambda <$ 0.9 $\mu$m). Light-absorbing impurities within the snow cause the greatest reductions in albedo for coarse-grained snow [*Warren and Wiscombe*, 1980]. This is illustrated in Figure 3, which shows the reduction in the spectral albedo when light-absorbing carbon is added to three semi-infinite snow layers with different effective radii. At shorter wavelengths, photons generally experience more scattering events and

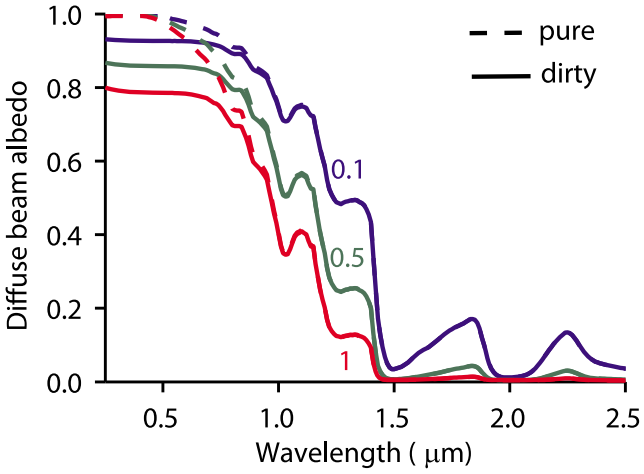


**Figure 3.** Semi-infinite diffuse beam albedo of pure (dashed) and dirty (solid) snow for three effective grain radii $r_e$ (mm). The dirty snow contains 0.3 ppmw of light-absorbing carbon.

travel a greater distance through the snow, increasing the probability that the photon will encounter an absorbing impurity and not re-emerge from the snowpack. As the effective grain radius of snow increases, the average travel path lengthens, further increasing the probability of encountering an absorbing impurity. For wavelengths $\lambda > 0.9$ $\mu$m, snow spectral albedo is negligibly influenced by the presence of impurities because the already strong absorption by ice at these wavelengths leads to short travel paths. Impurities located within ice grains (internal mixture) are 1.4 times as absorbent as impurities located in air (externally mixed) and can receive proportionally more incident radiation if located near the center of an ice sphere due to the refraction of light toward the sphere's center [*Chýlek et al.*, 1983; *Bohren*, 1986]. Impurities concentrated near the surface have a greater impact on albedo [*Aoki et al.*, 2000; *Grenfell et al.*, 2002]. Because impurities reduce the albedo at wavelengths where most of the downward solar flux occurs they can have a large impact on the overall energy budget of snow and ice.

[20] Shortwave infrared albedo is also influenced by the incident radiation's angle of incidence (Figure 4). At higher angles of incidence a photon will, on average, travel a path that is closer to the surface increasing its probability of experiencing a scattering event that will send it out of the snowpack (see Figure 11 of *Warren* [1982]). In addition, the effective radius of snow grains is often smaller near the surface (where snow is younger), so photons entering at high angles of incidence will experience more scattering events near the surface. This is enhanced by significant asymmetric scattering in the near-infrared region of $\lambda >$ 1.4 $\mu$m that strongly favors scattering in the forward direction [*Aoki et al.*, 2000; *Hudson et al.*, 2006]. Near-ultraviolet and visible wavelengths experience such low absorption that nearly all radiation at these wavelengths eventually scatters back out of the snow regardless of angle of incidence.

[21] Surface roughness can also affect surface albedo by decreasing the angle of incidence relative to a flat surface. This is because more incident radiation is absorbed by the slope facing the sun (lower angle of incidence) than by the slope facing away from it (higher angle of incidence). While

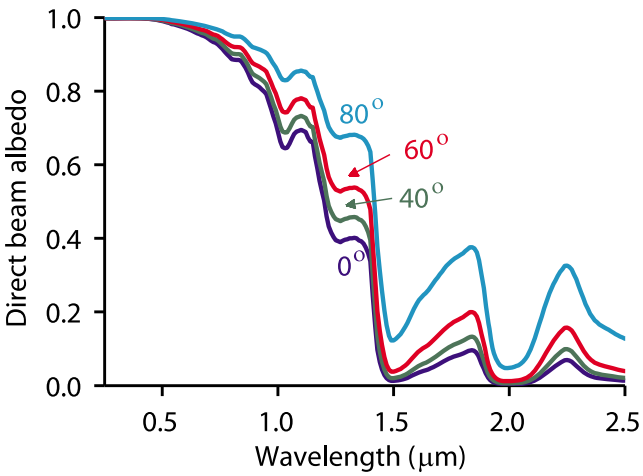


**Figure 4.** Semi-infinite direct beam albedo of pure snow ($r_e$ = 0.1 mm) as a function of solar zenith angle.

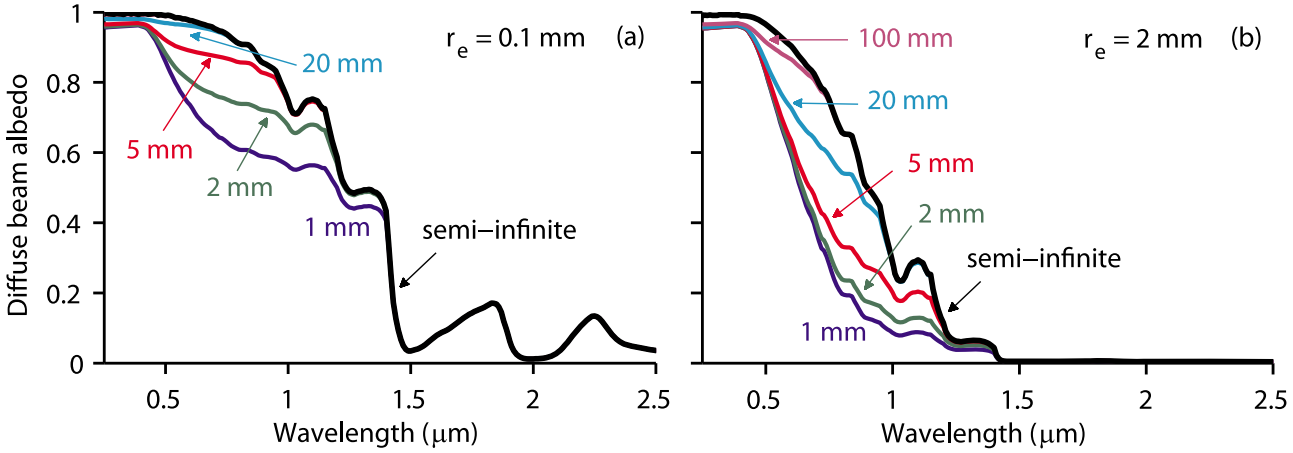


**Figure 5.** Semi-infinite diffuse beam albedo of pure white ice (contains air bubbles and has a clear sky broadband albedo of 0.40) overlain by a homogenous (a) fine- and (b) coarse-grained snow layer of varying thickness (mm w.e.).

surface roughness features can decrease the broadband albedo by as much as 4% at high solar zenith angles [*Carroll and Fitch*, 1981], this has little impact on the overall surface energy balance because little solar energy is received at high solar zenith angles and the fraction of direct incident radiation decreases with increasing solar zenith angle [*Warren et al.*, 1998].

[22] Snow is relatively absorptive in the near infrared, so, nearly all shortwave radiation with $\lambda > 1.5$ $\mu$m is absorbed within the top few millimeters of the snow. At near-ultraviolet and visible wavelengths scattering is high and absorption low, which allows radiation at these wavelengths to penetrate the snow to several meters depth. Where a homogeneous pure fine-grained snow layer overlies pure white ice with a broadband albedo of 0.4, surface albedo in the near-ultraviolet and visible parts of the spectrum is minimally affected by the presence of the underlying white ice when snow depths are >10 mm w.e., and completely unaffected in the shortwave infrared (Figure 5a). For very coarse snow, in which photons generally experience less scattering events per unit depth, the surface albedo is minimally affected when snow depths >100 mm w.e. (Figure 5b). Of course, the albedo of snow overlying a surface that is strongly absorbent in the near-ultraviolet and visible parts of the spectrum (soil, dirt, or snow with a high impurity content) will be much more sensitive to snow depth than that of snow overlying white ice.

[23] The optical properties of pure ice and water are very similar in the shortwave part of the spectrum, so the presence of liquid water in snow has little direct effect on snow albedo [*Dozier*, 1989; *Green et al.*, 2002]. Liquid water does however indirectly alter snow albedo by enhancing grain growth and infilling voids between snow grains, increasing the effective grain size [*Colbeck*, 1979]. The infilling of voids is the reason that saturated snow tends to have a lower albedo than unsaturated wet snow. Liquid water ponding on the surface of glaciers [*Zuo and Oerlemans*, 1996; *Greuell*, 2000; *Greuell et al.*, 2002] and sea ice [*Grenfell and Maykut*, 1977; *Perovich et al.*, 2002; *Light et al.*, 2008] can greatly reduce shortwave albedo and increase transmittance by reducing the number of air-ice boundaries that exist near the ice surface. Both observational [*Hanson*, 1965] and modeling studies [*Lüthje et al.*, 2006] have shown that ice ablation rates below surface ponds can be 2–3 times greater than on nearby bare ice.

[24] The albedo of glacier, lake and sea ice is influenced by the same factors as snow with the exception that, instead of being governed by grain size, the frequency and location of scattering events (air-ice interfaces) are determined by the size and distribution of air bubbles, brine inclusions and cracks within the ice [*Mullen and Warren*, 1988; *Askebjer et al.*, 1997; *Warren et al.*, 2002; *Light et al.*, 2003; *Ackermann et al.*, 2006]. In a pure ice sample that contains only air bubbles, all photon absorption events will occur within the ice and all scattering will occur at the ice-bubble boundaries (neglecting any surface reflection and internal scattering and absorption by interstitial air). Any size distribution of air bubbles within ice can be described by an effective bubble radius ($r_e'$) and an effective bubble concentration ($n_e'$) that has the same specific surface area ($\hat{S}$: cm$^2$ g$^{-1}$) as the population of bubbles of the ice that it describes [*Mullen and Warren*, 1988; *Warren et al.*, 2002]. An increase in either $r_e'$ or $n_e'$ causes an increase in the surface albedo at wavelengths $\lambda > 0.5$ $\mu$m. The influence of $r_e'$ on the surface albedo of ice with a constant $n_e'$ is shown in Figure 6.

### 3.2. Solar Irradiance

[25] As shortwave radiation passes through the earth's atmosphere it is modified by scattering, absorption and reflection. The shortwave irradiance incident upon the earth's surface is dependent on the solar zenith angle (Figure 7a), cloud optical thickness (Figure 7b), cloud amount, the transmission properties of the atmosphere, aerosol extinction, surface-atmosphere reflections (Figure 7c), surface slope and aspect, and shadowing and reflection by terrain.

[26] As discussed in the section 3.1, the spectral albedo of snow and ice is dependent on the angle of incidence of the incoming radiation (Figure 4). The effective angle of incidence is dependent on both the fraction of diffuse radiation and the zenith angle of the direct solar beam (Figure 7d). Under clear sky conditions the total incident

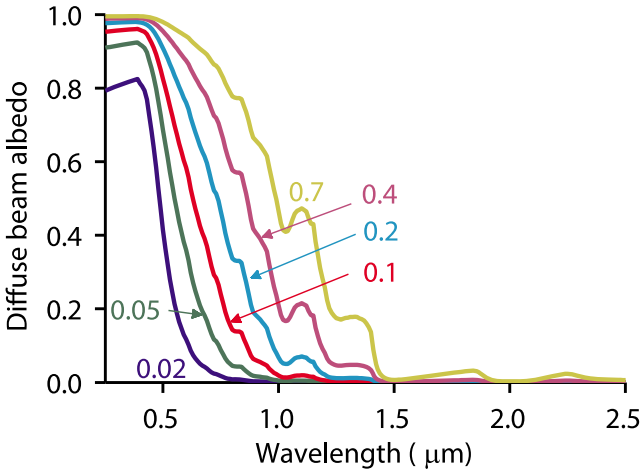


**Figure 6.** Semi-infinite diffuse beam albedo of pure ice as a function effective air bubble radius (mm) with a constant effective bubble concentration $n'_e$ = 0.3 mm$^{-3}$. Here 0.3 mm$^{-3}$ is the mean bubble concentration determined from 28 Greenland and Antarctica ice core samples [*Spencer et al.*, 2006].

radiation decreases as the solar zenith angle increases, and the fraction of diffuse irradiance increases due to an increase in the atmospheric path length (Figure 8a). Since diffuse radiation has an effective solar zenith angle of ~50° over a horizontal snow surface [*Warren*, 1982], the increase in spectral albedo of snow as the solar zenith angle increases is somewhat mitigated by an increase in the fraction of diffuse radiation.

[27] The fraction of diffuse radiation also increases with the presence of clouds (Figure 8b). Thus, when the sun is low on the horizon, cloud cover decreases the effective solar zenith angle relative to clear sky conditions. Clouds, which have similar optical properties to snow, also alter the spectral distribution of incident shortwave radiation by preferentially absorbing near-IR wavelengths and returning near-UV and visible wavelengths that have been reflected from the surface (Figure 7b). This increases the fraction of total shortwave radiation incident at shorter wavelengths where the albedo of snow is highest (Figure 2). In general, the net effect of the spectral shift toward shorter wavelengths and the increase in the diffuse faction of incident radiation results in an increase in the spectrally integrated albedo of snow and ice [*Grenfell and Maykut*, 1977; *Carroll*

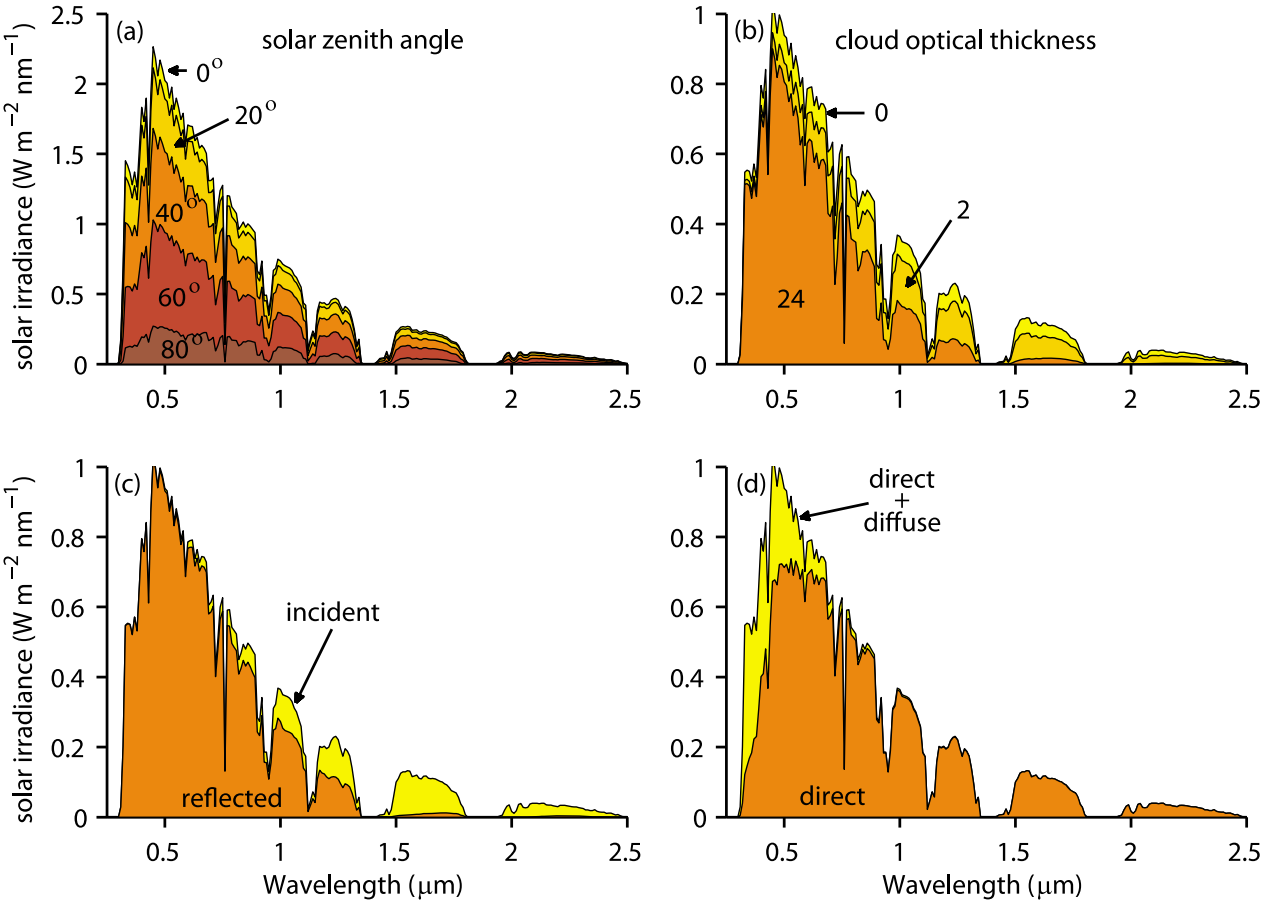


**Figure 7.** (a) Solar spectral irradiance for solar zenith angles between 0 and 80°, (b) cloud optical thicknesses of 0, 2, and 24 (this range in arctic cloud optical thickness was taken from *Curry et al.* [1996]), (c) incoming and reflected irradiance over a fresh snow surface, and (d) direct and diffuse spectral irradiance components. Figures 7a, 7c and 7d, are for clear sky conditions, and Figures 7b–7d are for a solar zenith angle of 60°. See text for details.

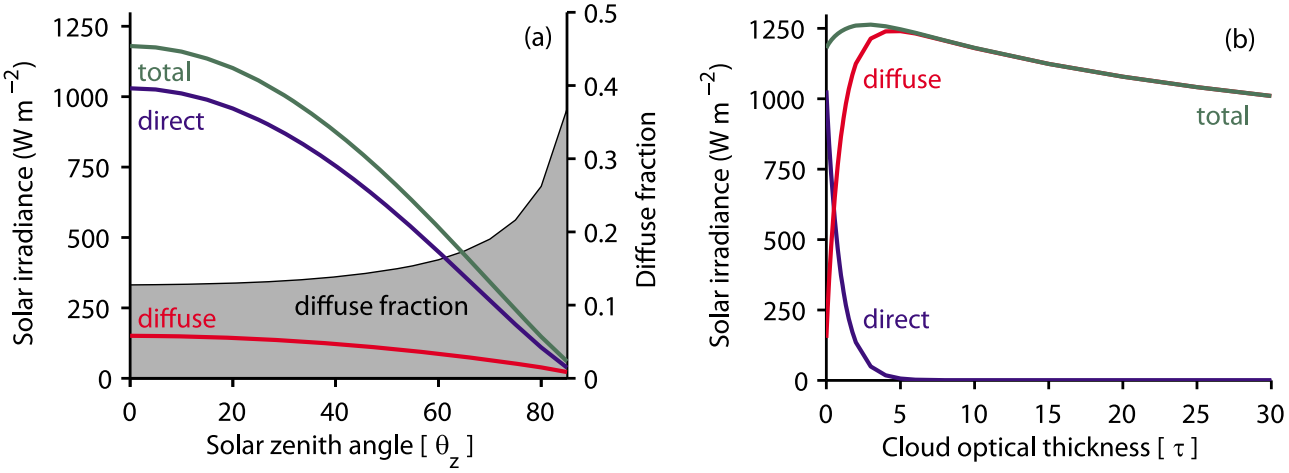


**Figure 8.** Total, direct, and diffuse solar irradiance. (a) Clear sky values as a function of solar zenith angle, and (b) cloud sky values for a solar zenith angle of 0° as a function of cloud optical thickness. See text for details.

*and Fitch*, 1981; *Grenfell and Perovich*, 1984; *Jonsell et al.*, 2003; *Grenfell and Perovich*, 2008].

## 4. Broadband Albedo of Snow and Ice and Its Parameterization

### 4.1. Theoretically Determined Broadband Albedos

[28] Broadband albedos determined with the snow and ice–atmosphere radiative transfer model show a nearly perfect logarithmic relationship with specific surface area ($\hat{S}$; Figure 9a) and an inverse logarithmic relationship with effective grain size ($r_e$; not shown). As shown by *Bohren* [1983], albedos are virtually identical for equivalent $\hat{S}$ regardless of whether the medium is modeled as an assemblage of independent spherical ice grains or as an assemblage of spherical air bubbles encased in ice. This is very important and highlights the significance of using $\hat{S}$ instead of $r_e$ and $r_e'$ for the modeling snow and ice albedo.

[29] The modification of broadband albedo due to the presence of light-absorbing carbon is dependent on its concentration and the $\hat{S}$ of the snow/ice in which it resides (Figure 9a). Snow/ice with higher $\hat{S}$ are less impacted by carbon loading because solar radiation, on average, has a shorter travel path within the medium.

[30] Under clear sky conditions, broadband albedos of both pure and contaminated snow/ice increase nonlinearly with an increase in the solar zenith angle ($\theta_Z$; Figure 9b). Snow/ice contaminated with light-absorbing carbon are most sensitive to changes in solar zenith angle. This is because the migration of scattering events toward the surface as the solar zenith angle increases results in less absorption in the ultraviolet and visible wavelengths by the carbon particles.

[31] The broadband albedo of snow/ice also increases with cloud optical thickness ($\tau$) due to a spectral shift in the incident solar irradiance toward shorter wavelengths (Figure 9c). For solar zenith angles $<\sim 50°$, this increase is enhanced by an increase in the diffuse fraction of incident solar irradiance. The varying sensitivities of broadband albedo to increasing cloud cover for different snow and ice types can be understood by examining the respective spectral albedos. Pure fresh snow with large $\hat{S}$ has a very high spectral albedo for wavelengths where the majority of incident solar radiation occurs (Figure 2). This means that a shift in the solar spectrum toward shorter wavelengths will have little impact on the broadband albedo. The opposite is true for pure snow/ice with low $\hat{S}$. In this case there is a much larger contrast between spectral albedos for wavelengths $>0.8\mu$m and $<0.8\mu$m (Figure 6), leading to larger sensitivities to cloud induced changes in the spectral distribution of the solar irradiance. Snow and ice containing significant amounts of light-absorbing carbon have much lower albedos at shorter wavelengths (Figure 3). This has two effects; it limits the number of surface cloud reflections and, in turn, reduces the spectral shift in incident solar radiation, and it reduces the contrast in the spectral albedo across the wavelengths at which most of the solar radiation is incident (flattens the spectral albedo curve).

### 4.2. Previously Proposed Parameterizations

[32] Where albedo values are unknown they are often modeled from one or more surrogate variables that include grain size, snow age, snow depth, snow density, melt rate, and air temperature [e.g., *Brun et al.*, 1992; *Brock et al.*, 2000; *Greuell*, 2000; *Klok et al.*, 2003]. Some of the more sophisticated empirical models also account for albedo modification due to impurity loading, solar zenith angle, and cloud cover [e.g., *Dickinson et al.*, 1986; *Marshall*, 1989; *Greuell and Konzelmann*, 1994]. Here we introduce a selection of published albedo parameterizations that will be compared to the snow and ice–atmosphere radiative transfer model (hereafter full model). As there are too many parameterizations to evaluate all of them, we focus the comparison on parameterizations that have been employed in the well established snow and ice metamorphism models CROCUS [*Brun et al.*, 1989], SOMARS [*Greuell and Konzelmann*, 1994], and SNTHERM [*Jordan*, 1991].

[33] Time-dependent albedo parameterizations such as those that are either linear [*Winther*, 1993], exponential [*Ranzi and Rossi*, 1991; *Klok and Oerlemans*, 2004], and/

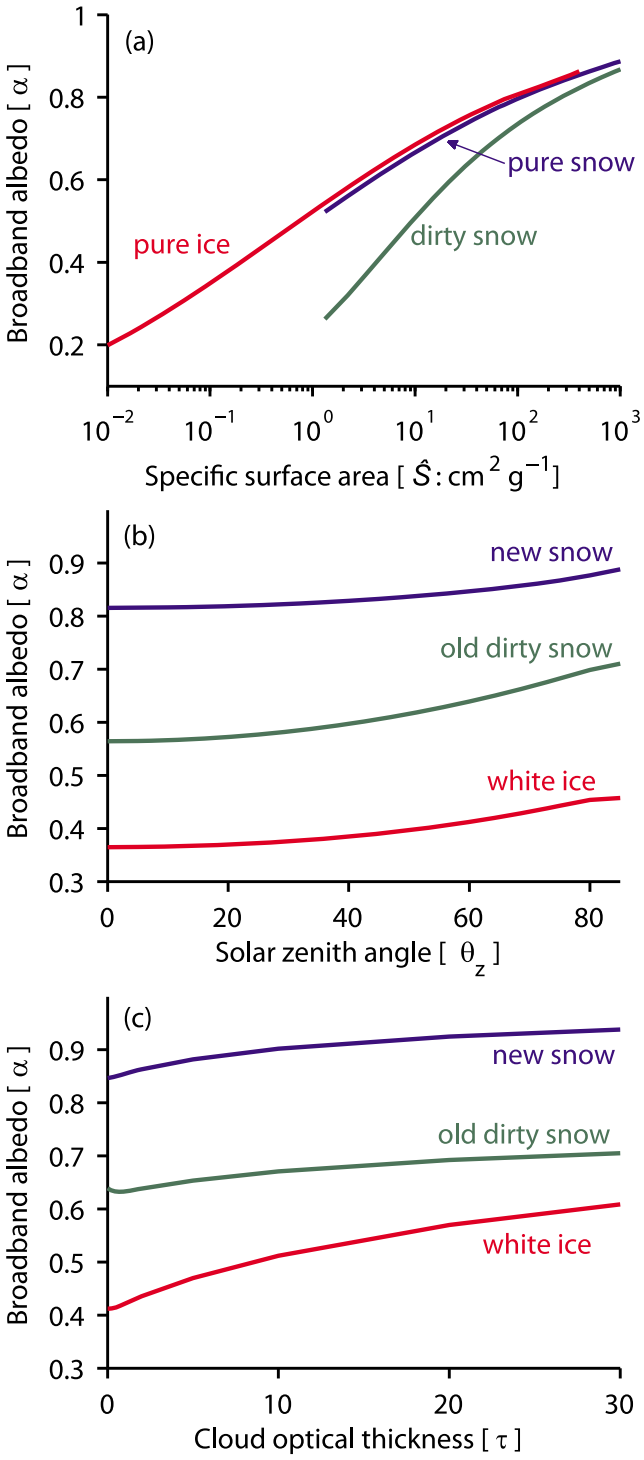


**Figure 9.** Semi-infinite broadband albedo of snow and ice as a function of (a) specific surface area ($\hat{S}$), (b) solar zenith angle, and (c) cloud optical thickness. "Dirty snow" contains 0.3 ppmw of light-absorbing carbon and "old dirty snow" contains the same amount of light-absorbing carbon and has an effective grain size $r_e$ = 1 mm. "New snow" values are for pure snow with $r_e$ = 0.1 mm. "White ice" values are for pure ice that has an effective bubble radius of $r'_e$ = 0.075 mm and an effective bubble concentration of $n'_e$ = 0.3 mm$^{-3}$.

or logarithmic [*Brock et al.*, 2000] functions of the temperature sum since the previous snowfall event or exponential time decay models [*Klok and Oerlemans*, 2004; *Bougamont and Bamber*, 2005], use simple proxies to model the time evolution of snow albedo. This is largely the result of snow grain metamorphism, and likely includes effects of time-dependent changes in grain size, impurity loading, snow depth, and atmospheric conditions. The theoretical broadband albedos and solar incidence calculated using the snow and ice–atmosphere radiative transfer model are specific to the physical characteristics of the snow and ice, the evolution of which must be simulated with a snow grain metamorphism model [*Marbouty*, 1980; *Brun*, 1989; *Legagneux et al.*, 2004; *Flanner and Zender*, 2006; *Taillandier et al.*, 2007]. To avoid the need to perform such simulations, we restrict our analysis to the comparison of full model results with those albedo parameterizations that are independent of time.

[34] The parameterizations we have selected for comparison are as follows:

[35] 1. A density-dependent albedo parameterization that was developed for use in the SOMARS snow and ice mass balance model [*Greuell and Konzelmann*, 1994]:

$$\alpha = \alpha_i + (\rho_{ss} - \rho_i)\left(\frac{\alpha_s - \alpha_i}{\rho_s - \rho_i}\right) \tag{1}$$

where $\alpha$ and $\rho$ are albedo and density and subscripts $i$, $s$ and $ss$ are for ice, fresh snow and surface snow. $\rho_s$ and $\rho_i$ are generally taken to be ~300 and ~910 kg m$^{-3}$, the densities of fresh snow and ice, respectively. $\alpha_s$ and $\alpha_i$ are constants that are often determined as part of the model tuning process. $\rho_{ss}$ is calculated using a snow densification model. This parameterization is no longer used in SOMARS and has been replaced with a parameterization that is a function of the length of time that the surface has been wet. This parameterization is, however, still frequently used elsewhere in the snowmelt and glacier mass balance modeling community [*Wright et al.*, 2005; *Bassford et al.*, 2006; *Wright et al.*, 2007] and adds diversity to our comparison.

[36] 2. The albedo parameterization developed by *Brun et al.* [1992] approximates snow albedo in three spectral ranges as a function of effective grain diameter $d_e$ (m) (updated parameterization provided by Jean-Marie Willemet, personal communication, 2008):

$$\alpha_{0.3-0.8\,\mu m} = \min\left[0.94,\ 0.96 - 1.58 d_e^{0.5}\right] \tag{2}$$

$$\alpha_{0.8-1.5\,\mu m} = 0.95 - 15.4 d_e^{0.5} \tag{3}$$

$$\alpha_{1.5-2.8\,\mu m} = 0.88 + 346.3 d'_e - 32.31 d'^{0.5}_e \text{ where } d'_e = \min[d_e,\ 0.0023] \tag{4}$$

This albedo scheme is part of the CROCUS snow model [*Brun et al.*, 1989] which has been used in numerous snow studies [e.g., *Martin et al.*, 1996; *Durand et al.*, 1999; *Lefebre et al.*, 2003] and has been coupled with the French ARPEGE global climate model [*Brun et al.*, 1997].

[37] 3. An albedo parameterization that accounts for changes in albedo with solar zenith angle. The parameterization used most commonly to account for these changes was proposed by *Dickinson et al.* [1986] for use in the Biosphere-Atmosphere Transfer Scheme (BATS):

$$\alpha = \alpha_{\theta_Z>60^\circ} + \max\left[0,\ 0.4\left(\frac{1-\alpha_{\theta_Z<60^\circ}}{b}\right)\left(\frac{b+1}{1+2bu}-1\right)\right] \tag{5}$$

where $u = \max \cos \theta_Z$, $\alpha_{\theta_Z > 60^\circ}$ is the constant snow albedo for solar zenith angles $\theta_Z$ less than 60°, $b$ is a tunable parameter used to fit modeled to observed data and $u'$ is the effective cosine of the solar zenith angle. If no observational data are available, $b$ is often set equal to 2 [*Segal et al.*, 1991; *Lefebre et al.*, 2003]. Albedos for zenith angles less than 60° are unchanged.

[38] 4. An albedo parameterization that accounts for observed changes in albedo with increasing cloud cover ($n_c$) that was originally proposed by for use in SOMARS [*Greuell and Konzelmann*, 1994]:

$$\alpha_{cloud} = \alpha_{clear} + 0.05(n_c - 0.5) \tag{6}$$

[39] 5. The physically based parameterization developed by *Marshall* [1989] that was developed by fitting piecewise equations to theoretical model output [*Warren and Wiscombe*, 1980; *Wiscombe and Warren*, 1980]. Marshall parameterized both visible and near-infrared albedos as a function of the square root of the effective grain radius and also accounted for the effects of solar zenith angle, soot contamination, and finite snow depth. This parameterization relies heavily on look-up tables and has been developed as a FORTRAN subroutine (SNOALB). This subroutine has been incorporated successfully into both regional and global climate models [*Marshall and Oglesby*, 1994; *Marshall et al.*, 1999; *Marshall et al.*, 2003]. A simplified adaptation of Marshall's parameterization is included in the SNTHERM snow model [*Jordan*, 1991], which is maintained by the U.S. Army Corps of Engineers, Cold Regions Research and Engineering Laboratory.

### 4.3. Comparison Between Theoretical Results and Selected Parameterizations

[40] Results from the five selected albedo parameterizations were compared with those from the full model:

[41] 1. Since the *Greuell and Konzelmann* [1994] albedo parameterization is based on density and not on effective grain size, the empirical relationship proposed by *Dominé et al.* [2007, equation (1)] was used to estimate snow density from the specific surface area of snow. In general, for $r_e <$ 2 mm, the Greuell and Konzelmann parameterization (equation (1)) underestimates the broadband albedo relative to full model results, with a maximum underestimation of 12% (Figure 10a).

[42] 2. The *Brun et al.* [1992] grain size–dependent albedo parameterization (equations (2)–(4)) does a good job of reproducing theoretical results for $r_e < 0.5$ mm but underestimates broadband albedos by as much as 15% relative to full model values for $r_e > 0.5$ mm (Figure 10a).

[43] 3. The *Dickinson et al.* [1986] parameterization (equation (5)) underestimates the theoretical increase in broadband albedo with increasing solar zenith angle by about 50% (Figure 10b). It does, however, do a good job of reproducing the increase in sensitivity of albedo to changes in the solar zenith angle as the effective radius of snow becomes larger.

[44] 4. Overall, the *Greuell and Konzelmann* [1994] parameterization, which simulates the broadband albedo response to changes in cloud optical thickness (equation (6)), produces a similar shaped albedo response as seen in the full model results but slightly overestimates the magnitude of the response (Figure 10c). In order to compare the Greuell and Konzelmann parameterization with full model results it was necessary to estimate cloud amount from cloud optical thickness using the relationship proposed by *Konzelmann et al.* [1994, equation (3)]. This introduces additional uncertainty into the comparison, as is shown by the gray shading in Figure 10c.

[45] 5. Last, full model predictions of broadband albedo were compared with predictions from the *Marshall* [1989] parameterization for different grain sizes (Figure 10a), solar zenith angles (Figure 10b) and cloud optical thicknesses (Figure 10c). Clear-sky broadband albedos determined with the Marshall parameterization for snow with $r_e \leq 0.7$ mm and solar zenith angles < 80° were well matched with full model results. As $r_e$ exceeded 0.8 mm and/or cloud cover increases the albedo is increasingly underpredicted. Comparisons between the Marshall parameterization and the full model were also made for snow contaminated with varying amounts of light absorbing carbon. This comparison showed similar deviations as were evident in the comparisons for pure snow.

[46] All five selected albedo parameterizations show varying degrees of disagreement with the full model results. Overall, the *Marshall* [1989] parameterization compares most favorably with the full model, but none of the parameterizations examined perform well for effective grain radii $r_e > 1$ mm or under cloudy sky conditions. The numerical details of the comparison between theoretical results and these selected parameterizations can be found in Appendix A.

### 4.4. A New Broadband Albedo Parameterization

[47] Here we develop a simple broadband albedo parameterization that closely matches full model results and is valid for a diverse array of snow, ice, and atmospheric conditions. The full model was run at a spectral resolution of 0.01 $\mu$m for the spectral range 0.2–4 $\mu$m, and for a wide range of semi-infinite homogeneous snow and ice media. Spectral snow surface albedos were determined for 352 snow types, defined by 22 effective ice grain radii between 0.025 and 5 mm and 16 light-absorbing carbon concentrations between 0 and 2 ppmw. This range of light-absorbing carbon concentrations covers the full range of published values [*Hansen and Nazarenko*, 2004]. Spectral ice surface albedos were determined for 192 ice types defined by 12 effective air bubble radii between 0.04 and 0.9 mm at an effective bubble concentration of 0.3 $mm^{-3}$ and 16 light-absorbing carbon concentrations. In total,

spectral albedos were calculated for 544 snow and ice types at 18 solar zenith angles between 0 and 85° and 11 cloud optical thicknesses ranging between 0 and 30. Integrating across the solar spectrum and dividing the total reflected irradiance by the total incident irradiance, 108 thousand broadband snow and ice albedos were determined. Atmospheric, snow and ice properties assigned to each model run are summarized in Table B1 of Appendix B.

[48] Pure snow and ice broadband albedos are asymptotically related to specific surface area ($\hat{S}$: cm$^2$ g$^{-1}$) and are nearly identical for equivalent specific surface areas of spherical ice grains and air bubbles (Figure 9a). For a solar zenith angle and cloud optical depth of zero, pure snow and ice broadband albedos ($\alpha_{\hat{S}}$) can be modeled accurately for specific surface areas in the range 0.07–1300 cm$^2$ g$^{-1}$ ($R^2$ = 0.997, standard error $S_e$ = 0.008, absolute maximum error $M_e$ = 0.02) using the simple asymptotic function

$$a_{\hat{S}} = 1.48 - \hat{S}^{-0.07} \tag{7}$$

The relationship between broadband snow and ice albedo and specific surface area changes as the concentration of light-absorbing carbon ($c$; ppmw) in the snow/ice increases (Figure 9a). The change in broadband snow and ice albedo due to loading by light-absorbing carbon from 0 to 2 ppmw ($d\alpha_c$) can be modeled using the equation ($R^2$ = 0.999, $S_e$ = 0.007, $M_e$ = 0.02):

$$da_c = \max\left(0.04 - a_{\hat{S}}, \frac{-c^{0.55}}{0.16 + 0.6\hat{S}^{0.5} + 1.8c^{0.6}\hat{S}^{-0.25}}\right) \tag{8}$$

where the broadband albedo of the loaded snow/ice is $\alpha_c = \alpha_{\hat{s}} + d\alpha_c$, if there are no impurities $\alpha_c = \alpha_{\hat{s}}$. The change in clear sky broadband snow and ice albedo with change in solar zenith angle ($d\alpha_{\theta_Z}$; Figure 9b) can be modeled using ($R^2$ = 0.997, $S_e$ = 0.007, $M_e$ = 0.03):

$$d\alpha_{\theta_Z} = 0.53\alpha_{\hat{S}}(1 - \alpha_c)(1 - u)^{1.2} \tag{9}$$

where $u$ is the cosine of the solar zenith angle.

[49] Next, a set of equations was developed that can reproduce the increase in broadband albedo of snow and ice resulting from an increase in cloud cover for clouds with optical thicknesses ranging between 0 and 30 (Figure 9c). The increase in the diffuse fraction of the incident radiation

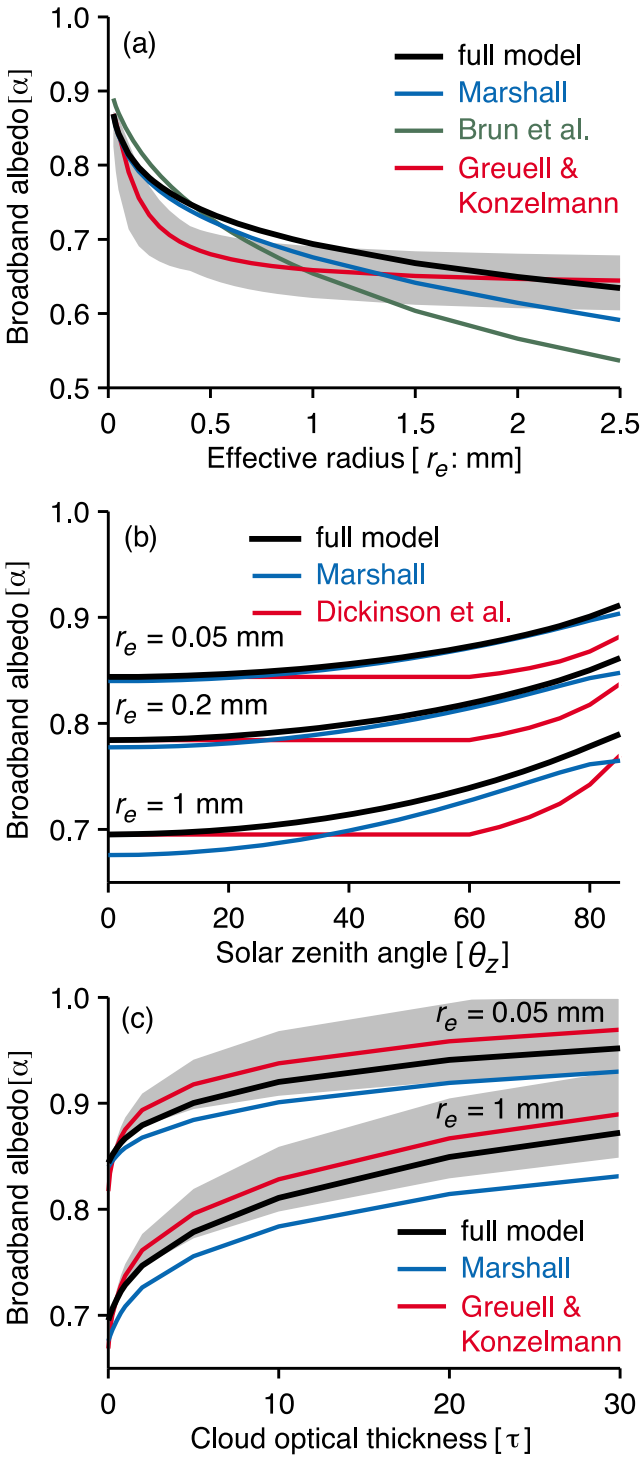


**Figure 10.** Results from five selected albedo parameterizations compared with those from the snow and ice–atmosphere radiative transfer model (full model): (a) Comparison between the *Marshall* [1989], *Brun et al.* [1992], and *Greuell and Konzelmann* [1994] parameterizations and full model results for varying effective grain radii ($r_e$) under clear sky conditions with $\theta_Z = 0°$. (b) Comparison between the *Marshall* [1989] and *Dickinson et al.* [1986] parameterization and full model results for clear sky conditions of varying $\theta_Z$. (c) Comparison between the *Marshall* [1989] and *Greuell and Konzelmann* [1994] albedo parameterizations and full model results for varying cloud optical thicknesses ($\tau$) with $\theta_Z$ = 0°. Shaded gray areas give the $\sigma$1 error in estimated broadband albedos resulting from (1) the use of estimated snow densities derived from known specific surface areas as input into the *Greuell and Konzelmann* [1994] density based albedo parameterization and (2) the use of estimated cloud amounts derived from known cloud optical thicknesses as input into the *Greuell and Konzelmann* [1994] parameterization of the influence of cloud on the albedo of snow. See text for details.

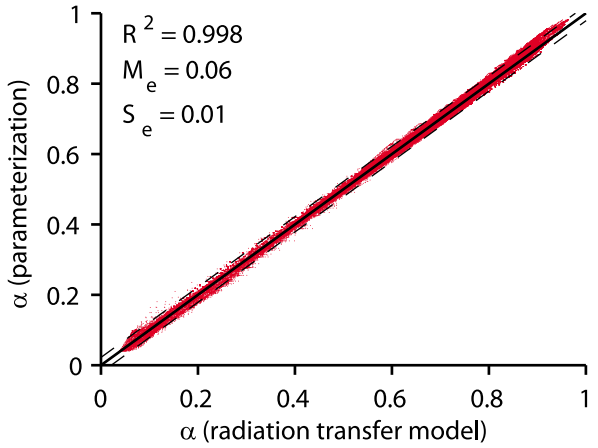


**Figure 11.** Broadband albedo of snow and ice ($\alpha$) determined from the snow and ice–atmosphere radiative transfer model compared with results from the newly proposed parameterization of snow and ice albedo (equations (7)–(12)). The solid black line shows the one-to-one relationship and the dashed lines give the 95% confidence levels.

as the cloud optical thickness increases from 0 to 3 can be approximated with a linear weighting function that adjusts the cosine of the effective solar zenith angle ($u'$) toward that of diffuse radiation ($\sim$50°) as both the cloud optical thickness and solar zenith angle increase:

$$u' = 0.64x + (1 - x)u \tag{10}$$

where $x = \min\left[\left(\frac{\tau}{3u}\right)^{0.5}, 1\right]$.

[50] Using $u'$ in equation (9), the additional change in broadband albedo due to the spectral shift in incident radiation caused by an increase in cloud optical thickness ($d\alpha_\tau$) can be modeled with ($R^2 = 0.998$, $S_e = 0.01$, $M_e = 0.06$):

$$d\alpha_\tau = \frac{0.1\tau\alpha_c^{1.3}}{(1 + 1.5\tau)^{\alpha_{\hat{S}}}} \tag{11}$$

The resultant broadband albedo ($\alpha$) is determined by summing all contributing components:

$$\alpha = \alpha_{\hat{S}} + d\alpha_c + d\alpha_{u'} + d\alpha_\tau \tag{12}$$

The newly proposed snow and ice albedo parameterization performs slightly better for snow with $r_e \leq 2$ mm and under clear sky conditions ($S_e = 0.006$, $M_e = 0.03$) than for snow, ice and atmospheric conditions outside of this range. That being said, deviations from full model results are minimal ($S_e = 0.01$, $M_e = 0.06$) under all 108 thousand modeled snow, ice, and atmosphere conditions (Figure 11).

[51] Equations (7)–(12) are for homogenous semi-infinite snow/ice. Because finite snow depth only impacts spectral albedos in the near-UV and visible [see *Wiscombe and Warren*, 1980, Figure 8], its effects are similar to adding or reducing the amount of light-absorbing carbon in semi-infinite snow. Therefore, the surface albedo for a finite snow layer of depth $z$ (m w.e.) overlying semi-infinite ice layer can be accounted for by replacing $d\alpha_c$ in equations (8)–(12) with a value which has been corrected for finite snow depth $d\alpha_c'$:

$$d\alpha_c' = \left(\alpha_c^{btm} - \alpha_s^{top}\right) + A\left(\alpha_c^{top} - \alpha_c^{btm}\right) \tag{13}$$

where $A = \min\left[1,\ 2.1z^{1.35\left(1-\alpha_{\hat{S}}^{top}\right)-0.1c^{top}-0.13}\right]$.

[52] The superscripts *top* and *btm* are for the upper and lower layers, respectively. Here $\alpha_{\hat{S}}^{top}$ and $d\alpha_c^{top}$ are determined for the overlying snow layer using equations (7) and (8). This equation compares very favorably ($R^2 = 0.985$, $S_e = 0.01$, $M_e = 0.07$) to a wide range of full model results for snow of varying depth overlying an ice layer of semi-infinite depth. Table B2 in Appendix B provides details of the full model runs to which the parameterization was fit. Equation (13) is only valid for snow overlying ice or old snow. Expanding the equation to account for finite snow depth over other surfaces, such as bare soil or vegetation, should be achievable by modeling the subsurface as an optically equivalent layer of dirty ice. Also note that equations (7)–(13) are only valid over the range of snow, ice and atmospheric conditions for which they have been developed (see Appendix B).

## 5. Discussion

[53] We have not yet had the opportunity to conduct a field campaign to collect measurements of the spectral albedo of snow and ice, solar spectral irradiance and snow properties to compare with our model results, therefore, we look to previous studies which have compared snow albedo measurements to results produced with multilayer plane-parallel radiative transfer models similar to the one employed in this study. Three such studies [*Grenfell et al.*, 1994; *Aoki et al.*, 2000; *Painter et al.*, 2007] all show very good agreement between theoretically modeled and observed snow spectral albedos when the snow stratigraphy is well known and the instrumentation is not left unattended. In addition, *Grenfell and Perovich* [2008] show exceptional agreement between incident solar spectral irradiance modeled using SBDART and observed values obtained over Arctic Ocean sea ice for a wide variety of atmospheric conditions using the same sub-Arctic atmospheric profile used in this study.

[54] The parameterization presented here accurately reproduces theoretical results under a wide range of snow and ice conditions, is computationally simple and requires, at most, five input parameters: snow/ice specific surface area, concentration of light-absorbing carbon, solar zenith angle, cloud optical thickness, and snow depth. Inputs can be determined from measurements and/or numerical model output. Snow specific surface areas can be measured directly using contact spectroscopy [*Painter et al.*, 2007], methane adsorption [*Dominé et al.*, 2001; *Legagneux et al.*, 2002], photographic methods [*Matzl and Schneebeli*, 2006], image analysis [*Sergent et al.*, 1993; *Sergent et al.*, 1998] and stereological techniques [*Davis and Dozier*, 1989], or

estimated from measurements of snow density and grain type [*Dominé et al.*, 2007]. Specific surface area can also be modeled using dry [*Marbouty*, 1980; *Legagneux et al.*, 2003; *Flanner and Zender*, 2006; *Taillandier et al.*, 2007] and wet [*Brun*, 1989] snow metamorphism models that are forced with the vertical temperature gradient, snow density and liquid water content, quantities that are often modeled within snow and climate models. Carbon concentrations can be determined from field measurements [*Clarke and Noone*, 1985] or from climate models that resolve carbon aerosol transport [*Flanner et al.*, 2007]. The solar zenith angle can be calculated from the latitude, solar declination angle, and time of day, and cloud optical thickness can be determined by comparing theoretical clear sky to observed solar irradiance, from satellite observations [*Platnick et al.*, 2003], statistically applied climatology [*Curry and Ebert*, 1992], or climate model output.

[55] Physically based parameterizations of snow and ice albedo offer the opportunity to better assess the impacts of changing environmental conditions on the energy budget of snow and ice. These will not be as easy to evaluate using empirical albedo parameterizations based on measurements of site specific snow, ice and atmospheric conditions. The new broadband albedo parameterization proposed here reproduces theoretical results very well when the exact snow, ice, and atmosphere properties are known. However, for use in energy balance, melt or climate models this parameterization will, at a minimum, require input of snow grain radii from a snow grain growth model. In practical terms, the proposed albedo parameterization will only be as accurate as the snow grain growth model with which it is forced. Recently there has been a renewed effort toward the improvement of such models [*Legagneux et al.*, 2003; *Flanner and Zender*, 2006; *Taillandier et al.*, 2007] but much work is still needed to confirm their validity over a wide range of environmental conditions.

## 6. Summary

[56] The spectral albedo of snow and ice is the net result of many reflections and refraction of shortwave radiation at air-ice boundaries, and its absorption as it passes though ice and comes into contact with light-absorbing impurities. The relative number of air-ice boundaries per unit mass of ice is dependent on the specific surface area of the medium. A smaller specific surface area will, on average, result in a lower number of scattering events and longer travel paths of shortwave radiation within snow and ice, leading to lower surface albedos. Addition of light-absorbing impurities increases the probability of absorption, further reducing albedo. It is not only the characteristics of the snow/ice that govern its albedo, but also the angle of incidence (solar zenith angle and diffuse fraction of incident radiation) and, in the case of broadband albedo, the spectral distribution of the incident shortwave radiation.

[57] The responses of broadband albedo to changes in specific surface area, impurity loading, angle of incidence, or spectral distribution and diffuse fraction of incident shortwave radiation are highly interdependent. Multiple reflections between the surface and clouds generate an interdependence between surface albedo and the spectral distribution of incident radiation. This necessitates the use of coupled snow and ice–atmosphere radiative transfer models to model broadband albedos. However, such models can be computationally expensive and difficult to implement in existing energy mass balance and climate models.

[58] Comparisons between selected preexisting parameterizations of snow albedo and a coupled snow and ice–atmosphere radiative transfer model show varying degrees of disagreement. In response, we have developed a new parameterization of broadband albedo that accurately reproduces theoretical results under a wide range of snow and ice conditions. It is computationally simple and requires between one and five input parameters, depending on its application. These parameters are specific surface area of snow/ice, concentration of light-absorbing carbon, solar zenith angle, cloud optical thickness, and snow depth. More work is needed to assess the performance of existing snow grain growth models which are required to provide input to such an albedo parameterization in energy balance and climate models.

## Appendix A: Comparison Between Theoretical Results and Selected Parameterizations: Numerical Details

[59] The parameterizations of *Brun et al.* [1992] and *Marshall* [1989] both model albedo in more than one spectral band. To determine broadband albedos, these parameterizations require weightings of the solar irradiance incident in each of the spectral bands. In addition, the *Marshall* [1989] parameterization requires values of the diffuse fraction and atmospheric transmittance. To provide an objective comparison with full model results, irradiance weightings, diffuse fractions and atmospheric transmittance values for each spectral band were taken directly from the full model.

[60] Uncertainties associated with using the *Dominé et al.*'s [2007, equation (1)] approximation to estimate density from specific surface area for use by the *Greuell and Konzelmann* [1994] parameterization were determined by adjusting the known specific surface areas by ±62% (the $1\sigma$ error) [*Dominé et al.*, 2007] and setting a minimum error

**Table B1.** Specifications of the 108 Thousand Model Runs for Semi-infinite Snow/Ice Depth

| Property | Values | Units |
|---|---|---|
| | *Atmosphere* | |
| $\theta_Z$ | 0, 5, 10, 15, 20, 25, 30, 35, 40, 45, 50, 55, 60, 65, 70, 75, 80, 85 | degrees |
| $\tau$ | 0, 0.1, 0.25, 0.5, 0.75, 1, 2, 5, 10, 20, 30 | no units |
| | *Snow* | |
| $r_e$ | 0.025, 0.0375, 0.05,0.1, 0.15, 0.2, 0.25, 0.3, 0.35, 0.4, 0.45, 0.5, 0.6, 0.7, 0.8, 0.9, 1, 1.5, 2, 2.5, 5 | mm |
| $c$ | 0, 0.002, 0.004, 0.006, 0.01, 0.015, 0.02, 0.04, 0.06, 0.08, 0.1, 0.2, 0.3, 0.5, 1, 2 | ppmw |
| | *Ice* | |
| $n'_e$ | 0.3 | $mm^{-3}$ |
| $r'_e$ | 0.04, 0.05, 0.075, 0.1, 0.2, 0.3, 0.4, 0.5, 0.6, 0.7, 0.8, 0.9 | mm |
| $c$ | 0, 0.002, 0.004, 0.006, 0.01, 0.015, 0.02, 0.04, 0.06, 0.08, 0.1, 0.2, 0.3, 0.5, 1, 2 | ppmw |

**Table B2.** Specifications of the 24 Thousand Model Runs for a Single Snow Layer of Depth $z$ Overlying a Semi-infinite Ice Layer

| Property | Values | Units |
|---|---|---|
| | *Atmosphere* | |
| $\theta_Z$ | 0, 35, 75 | degrees |
| $\tau$ | 0, 1, 2, 5, 10, 20 | no units |
| | *Snow* | |
| $r_e$ | 0.05, 0.15, 0.45, 1 | mm |
| $c$ | 0, 0.2, 0.1, 0.3 | ppmw |
| $z$ | 0.01, 0.03, 0.05, 0.09, 0.25, 0.5, 5 | m w.e. |
| | *Ice* | |
| $n'_e$ | 0.3 | $mm^{-3}$ |
| $r'_e$ | 0.05, 0.3, 0.7 | mm |
| $c$ | 0, 0.2, 0.1, 0.3 | ppmw |

of $\pm 50$ $cm^2$ $g^{-1}$ for specific surface areas smaller than 80 $cm^2$ $g^{-1}$ (approximated from *Dominé et al.*'s [2007] Figure 1). The tunable parameters for the Greuell and Konzelmann parameterization (equation (1)) of new snow albedo ($\alpha_S$ = 0.84) and density ($\rho_s$ = 0.01 g $cm^{-3}$) were assigned values determined by the full model for snow with an effective radius of $r_e$ = 0.05 mm. As with most other applications of the *Dickinson et al.* [1986] parameterization (equation (5)), the coefficient $b$ is set equal to 2.

[61] Parameterizations were only compared with full model results for 0.05 mm $\leq r_e \leq$ 2.5 mm. This is the range of effective radii for which the *Brun et al.* [1992] and *Marshall* [1989] parameterizations were developed and is approximately the range over which the density-specific surface area approximation [*Dominé et al.*, 2007, equation (1)] is valid which was used to derive densities for input into the *Greuell and Konzelmann* [1994] parameterization.

## Appendix B: Model Run Specifications

[62] This appendix provides the atmospheric, snow, and ice properties assigned to the coupled snow and ice–atmosphere radiative transfer model for the determination of broadband snow and ice albedos. Table B1 provides the properties of the 108,000 homogenous semi-infinite depth snow and ice broadband albedos to which equations (7)–(11) were fit. Table B2 provides the specifications of the 24,000 latter broadband albedos to which equation (13) was fit. These broadband albedo values are for a homogenous finite depth snow layer overlying a homogenous semi-infinite depth ice layer.

[63] **Acknowledgments.** We thank Stephen Warren and Richard Brandt for their advice and for supplying tables of the optical constants of ice, Brian Toon for his helpful discussion of the numerical details of two-stream radiative transfer modeling, and Mark Flanner for making available his dry snow metamorphism model. We also thank Stephen Warren and an anonymous reviewer for their helpful comments. This work was supported by NSERC Canada, the Alberta Ingenuity Fund, and the Canadian Foundation for Climate and Atmospheric Sciences through the Polar Climate Stability Network. The work was conducted using the infrastructure and resources of AICT (Academic Information and Communication Technologies) of the University of Alberta.

## References

Ackermann, M., et al. (2006), Optical properties of deep glacial ice at the South Pole, *J. Geophys. Res.*, *111*, D13203, doi:10.1029/2005JD006687.

Aoki, T., T. Aoki, M. Fukabori, A. Hachikubo, Y. Tachibana, and F. Nishio (2000), Effects of snow physical parameters on spectral albedo and bidirectional reflectance of snow surface, *J. Geophys. Res.*, *105*, 10,219–10,236.

Askebjer, P., et al. (1997), Optical properties of deep ice at the South Pole: Absorption, *Appl. Opt.*, *36*, 4168–4180, doi:10.1364/AO.36.004168.

Bassford, R. P., M. J. Siegert, J. A. Dowdeswell, J. Oerlemans, A. F. Glazovsky, and Y. Y. Macheret (2006), Quantifying the mass balance of ice caps on Severnaya Zemlya, Russian High Arctic. I: Climate and mass balance of the Vavilov Ice Cap, *Arct. Antarct. Alp. Res.*, *38*, 1–12, doi:10.1657/1523-0430(2006)038[0001:QTMBOI]2.0.CO;2.

Bohren, C. F. (1983), Colors of snow, frozen waterfalls, and icebergs, *J. Opt. Soc. Am.*, *73*, 1646–1652, doi:10.1364/JOSA.73.001646.

Bohren, C. F. (1986), Applicability of effective-medium theories to problems of scattering and absorption by nonhomogeneous atmospheric particles, *J. Atmos. Sci.*, *43*, 468–475, doi:10.1175/1520-0469(1986)043<0468:AOEMTT>2.0.CO;2.

Bohren, C. F., and D. R. Huffman (1998), *Absorption and Scattering of Light by Small Particles*, 544 pp., Wiley-Intersci., New York.

Bond, T. C., and R. W. Bergstrom (2006), Light absorption by carbonaceous particles: An investigative review, *Aerosol Sci. Technol.*, *40*, 27–67, doi:10.1080/02786820500421521.

Bougamont, M., and J. L. Bamber (2005), A surface mass balance model for the Greenland Ice Sheet, *J. Geophys. Res.*, *110*, F04018, doi:10.1029/2005JF000348.

Brock, B. W., I. C. Willis, and M. J. Sharp (2000), Measurement and parameterization of albedo variations at Haut Glacier d'Arolla, Switzerland, *J. Glaciol.*, *46*, 675–688, doi:10.3189/172756500781832675.

Brun, E. (1989), Investigation on wet-snow metamorphism in respect of liquid-water content, *Ann. Glaciol.*, *13*, 22–26.

Brun, E., E. Martin, V. Simon, C. Gendre, and C. Coleou (1989), An energy and mass model of snow cover suitable for operational avalanche forecasting, *J. Glaciol.*, *35*, 333–342.

Brun, E., P. David, M. Sudul, and G. Brunot (1992), A numerical model to simulate snow-cover stratigraphy for operational avalanche forecasting, *J. Glaciol.*, *38*, 13–22.

Brun, E., E. Martin, and V. Spiridonov (1997), Coupling a multi-layered snow model with a GCM, *Ann. Glaciol.*, *25*, 66–72.

Carroll, J. J., and B. W. Fitch (1981), Effects of solar elevation and cloudiness on snow albedo at the South Pole, *J. Geophys. Res.*, *86*, 5271–5276.

Cess, R. D., et al. (1991), Interpretation of snow-climate feedback as produced by 17 general-circulation models, *Science*, *253*, 888–892, doi:10.1126/science.253.5022.888.

Chýlek, P., V. Ramaswamy, and V. Srivastava (1983), Albedo of soot-contaminated snow, *J. Geophys. Res.*, *88*, 837–843.

Clarke, A. D., and K. J. Noone (1985), Soot in the Arctic snowpack: A cause for perturbations in radiative transfer, *Atmos. Environ.*, *19*, 2045–2053, doi:10.1016/0004-6981(85)90113-1.

Colbeck, S. C. (1979), Grain clusters in wet snow, *J. Colloid Interface Sci.*, *72*, 371–384, doi:10.1016/0021-9797(79)90340-0.

Curry, J. A., and E. E. Ebert (1992), Annual cycle of radiation fluxes over the Arctic Ocean: Sensitivity to cloud optical properties, *J. Clim.*, *5*, 1267–1280, doi:10.1175/1520-0442(1992)005<1267:ACORFO>2.0.CO;2.

Curry, J. A., W. B. Rossow, D. Randall, and J. L. Schramm (1996), Overview of Arctic cloud and radiation characteristics, *J. Clim.*, *9*, 1731–1764, doi:10.1175/1520-0442(1996)009<1731:OOACAR>2.0.CO;2.

Davis, R., and J. Dozier (1989), Stereological characterization of dry alpine snow for microwave remote sensing, *Adv. Space Res.*, *9*, 245–251, doi:10.1016/0273-1177(89)90492-4.

Dickinson, R. E., A. Henderson-Sellers, P. J. Kennedy, and M. F. Wilson (1986), Biosphere-Atmosphere Transfer Scheme (BATS) for the NCAR Community Climate Model, *Tech. Note 275*, Natl. Cent. for Atmos. Res., Boulder, Colo.

Dominé, F., A. Cabanes, A.-S. Taillandier, and L. Legagneux (2001), Specific surface area of snow samples determined by CH4 adsorption at 77 K and estimated by optical microscopy and scanning electron microscopy, *Environ. Sci. Technol.*, *35*, 771–780, doi:10.1021/es001168n.

Dominé, F., A. S. Taillandier, and W. R. Simpson (2007), A parameterization of the specific surface area of seasonal snow for field use and for models of snowpack evolution, *J. Geophys. Res.*, *112*, F02031, doi:10.1029/2006JF000512.

Dozier, J. (1989), Spectral signature of alpine snow cover from the Landsat Thematic Mapper, *Remote Sens. Environ.*, *28*, 9–22, doi:10.1016/0034-4257(89)90101-6.

Durand, Y., G. Giraud, E. Brun, L. Merindol, and E. Martin (1999), A computer-based system simulating snowpack structures as a tool for regional avalanche forecasting, *J. Glaciol.*, *45*, 469–484.

Fitzpatrick, M. F., R. E. Brandt, and S. G. Warren (2004), Transmission of solar radiation by clouds over snow and ice surfaces: A parameterization in terms of optical depth, solar zenith angle, and surface albedo, *J. Clim.*, *17*, 266–275, doi:10.1175/1520-0442(2004)017<0266:TOSRBC>2.0.CO;2.

Flanner, M. G., and C. S. Zender (2006), Linking snowpack microphysics and albedo evolution, *J. Geophys. Res.*, *111*, D12208, doi:10.1029/2005JD006834.

Flanner, M. G., C. S. Zender, J. T. Randerson, and P. J. Rasch (2007), Present-day climate forcing and response from black carbon in snow, *J. Geophys. Res.*, *112*, D11202, doi:10.1029/2006JD008003.

Green, R. O., J. Dozier, D. Roberts, and T. Painter (2002), Spectral snow-reflectance models for grain-size and liquid-water fraction in melting snow for the solar-reflected spectrum, *Ann. Glaciol.*, *34*, 71–73, doi:10.3189/172756402781817987.

Grenfell, T. C. (1991), A radiative transfer model for sea ice with vertical structure variations, *J. Geophys. Res.*, *96*, 16,991–17,001, doi:10.1029/91JC01595.

Grenfell, T. C., and G. A. Maykut (1977), The optical properties of ice and snow in the Arctic Basin, *J. Glaciol.*, *18*, 445–463.

Grenfell, T. C., and D. K. Perovich (1984), Spectral albedos of sea ice and incident solar irradiance in the southern Beaufort Sea, *J. Geophys. Res.*, *89*, 3573–3580, doi:10.1029/JC089iC03p03573.

Grenfell, T. C., and D. K. Perovich (2008), Incident spectral irradiance in the Arctic Basin during the summer and fall, *J. Geophys. Res.*, *113*, D12117, doi:10.1029/2007JD009418.

Grenfell, T. C., and S. G. Warren (1999), Representation of a nonspherical ice particle by a collection of independent spheres for scattering and absorption of radiation, *J. Geophys. Res.*, *104*, 31,697–31,709.

Grenfell, T. C., D. K. Perovich, and J. A. Ogren (1981), Spectral albedos of an alpine snowpack, *Cold Reg. Sci. Technol.*, *4*, 121–127, doi:10.1016/0165-232X(81)90016-1.

Grenfell, T. C., S. G. Warren, and P. C. Mullen (1994), Reflection of solar-radiation by the Antarctic snow surface at ultraviolet, visible, and near-infrared wavelengths, *J. Geophys. Res.*, *99*, 18,669–18,684.

Grenfell, T. C., B. Light, and M. Sturm (2002), Spatial distribution and radiative effects of soot in the snow and sea ice during the SHEBA experiment, *J. Geophys. Res.*, *107*(C10), 8032, doi:10.1029/2000JC000414.

Grenfell, T. C., S. P. Neshyba, and S. G. Warren (2005), Representation of a nonspherical ice particle by a collection of independent spheres for scattering and absorption of radiation: 3. Hollow columns and plates, *J. Geophys. Res.*, *110*, D17203, doi:10.1029/2005JD005811.

Greuell, W. (2000), Melt-water accumulation on the surface of the Greenland Ice Sheet: Effect on albedo and mass balance, *Geogr. Ann., Ser. A*, *82*, 489–498, doi:10.1111/j.0435-3676.2000.00136.x.

Greuell, W., and T. Konzelmann (1994), Numerical modeling of the energy balance and the englacial temperature of the Greenland Ice Sheet: Calculations for the ETH-Camp Location (west Greenland, 1155 m a.s.l.), *Global Planet. Change*, *9*, 91–114, doi:10.1016/0921-8181(94)90010-8.

Greuell, W., C. H. Reijmer, and J. Oerlemans (2002), Narrowband-to-broadband albedo conversion for glacier ice and snow based on aircraft and near-surface measurements, *Remote Sens. Environ.*, *82*, 48–63, doi:10.1016/S0034-4257(02)00024-X.

Hansen, J., and L. Nazarenko (2004), Soot climate forcing via snow and ice albedos, *Proc. Natl. Acad. Sci. U. S. A.*, *101*, 423–428, doi:10.1073/pnas.2237157100.

Hansen, J. E., and L. D. Travis (1974), Light-scattering in planetary atmospheres, *Space Sci. Rev.*, *16*, 527–610, doi:10.1007/BF00168069.

Hanson, A. M. (1965), Studies of the mass budget of Arctic pack ice floes, *J. Glaciol.*, *5*, 701–709.

Horvath, H. (1993), Atmospheric light absorption: A review, *Atmos. Environ., Part A*, *27*, 293–317, doi:10.1016/0960-1686(93)90104-7.

Hudson, S. R., S. G. Warren, R. E. Brandt, T. C. Grenfell, and D. Six (2006), Spectral bidirectional reflectance of Antarctic snow: Measurements and parameterization, *J. Geophys. Res.*, *111*, D18106, doi:10.1029/2006JD007290.

Jonsell, U., R. Hock, and B. Holmgren (2003), Spatial and temporal variations in albedo on Storglaciaren, Sweden, *J. Glaciol.*, *49*, 59–68, doi:10.3189/172756503781830980.

Jordan, R. (1991), A one-dimensional temperature model for a snow cover, *Tech. doc. SNTHERM 89*, 49 pp., Cold Reg. Res. and Eng. Lab., Hanover, N. H.

Klok, E. J., and J. Oerlemans (2004), Modelled climate sensitivity of the mass balance of Morteratschgletscher and its dependence on albedo parameterization, *Int. J. Climatol.*, *24*, 231–245, doi:10.1002/joc.994.

Klok, E. J., W. Greuell, and J. Oerlemans (2003), Temporal and spatial variation of the surface albedo of Morteratschgletscher, Switzerland, as derived from 12 Landsat images, *J. Glaciol.*, *49*, 491–502, doi:10.3189/172756503781830395.

Konzelmann, T., R. S. W. Vandewal, W. Greuell, R. Bintanja, E. A. C. Henneken, and A. Abeouchi (1994), Parameterization of global and long-wave incoming radiation for the Greenland Ice Sheet, *Global Planet. Change*, *9*, 143–164, doi:10.1016/0921-8181(94)90013-2.

Lefebre, F., H. Gallee, J. P. van Ypersele, and W. Greuell (2003), Modeling of snow and ice melt at ETH Camp (west Greenland): A study of surface albedo, *J. Geophys. Res.*, *108*(D8), 4231, doi:10.1029/2001JD001160.

Legagneux, L., A. Cabanes, and F. Dominé (2002), Measurement of the specific surface area of 176 snow samples using methane adsorption at 77 K, *J. Geophys. Res.*, *107*(D17), 4335, doi:10.1029/2001JD001016.

Legagneux, L., T. Lauzier, F. Domin, W. F. Kuhs, T. Heinrichs, and K. Techmer (2003), Rate of decay of specific surface area of snow during isothermal experiments and morphological changes studied by scanning electron microscopy, *Can. J. Phys.*, *81*, 459–468, doi:10.1139/p03-025.

Legagneux, L., A.-S. Taillandier, and F. Domine (2004), Grain growth theories and the isothermal evolution of the specific surface area of snow, *J. Appl. Phys.*, *95*, 6175–6184, doi:10.1063/1.1710718.

Light, B., G. A. Maykut, and T. C. Grenfell (2003), Effects of temperature on the microstructure of first-year Arctic sea ice, *J. Geophys. Res.*, *108*(C2), 3051, doi:10.1029/2001JC000887.

Light, B., T. C. Grenfell, and D. K. Perovich (2008), Transmission and absorption of solar radiation by Arctic sea ice during the melt season, *J. Geophys. Res.*, *113*, C03023, doi:10.1029/2006JC003977.

Lüthje, M., L. T. Pedersen, N. Reeh, and W. Greuell (2006), Modelling the evolution of supraglacial lakes on the west Greenland Ice Sheet margin, *J. Glaciol.*, *52*, 608–618, doi:10.3189/172756506781828386.

Male, D. H., and R. J. Granger (1981), Snow surface energy exchange, *Water Resour. Res.*, *17*, 609–627, doi:10.1029/WR017i003p00609.

Marbouty, D. (1980), An experimental study of temperature-gradient metamorphism, *J. Glaciol.*, *26*, 303–312.

Marshall, S. E. (1989), A physical parameterization of snow albedo for use in climate models, *Coop. Thesis 123*, Natl. Cent. for Atmos. Res., Boulder, Colo.

Marshall, S., and R. J. Oglesby (1994), An improved snow hydrology for GCMs. Part 1: Snow cover fraction, albedo, grain size, and age, *Clim. Dyn.*, *10*, 21–37.

Marshall, S., R. J. Oglesby, K. A. Maasch, and G. T. Bates (1999), Improving climate model representations of snow hydrology, *Environ. Model. Software*, *14*, 327–334, doi:10.1016/S1364-8152(98)00084-X.

Marshall, S., R. J. Oglesby, and A. W. Nolin (2003), The predictability of winter snow cover over the western United States, *J. Clim.*, *16*, 1062–1073, doi:10.1175/1520-0442(2003)016<1062:TPOWSC>2.0.CO;2.

Martin, E., B. Timbal, and E. Brun (1996), Downscaling of general circulation model outputs: Simulation of the snow climatology of the French Alps and sensitivity to climate change, *Clim. Dyn.*, *13*, 45–56, doi:10.1007/s003820050152.

Matzl, M., and M. Schneebeli (2006), Measuring specific surface area of snow by near-infrared photography, *J. Glaciol.*, *52*, 558–564, doi:10.3189/172756506781828412.

Mätzler, C. (2002), MATLAB functions for Mie scattering and absorption, Version 2, *Rep. 2002–11*, Inst. für Angewandte Phys., 20 pp.

McClatchey, R. A., R. W. Fenn, J. E. A. Selby, F. E. Volz, and J. S. Garing (1972), Optical properties of the atmosphere, 3rd ed., *Rep. AFCRL-72-0497*, Air Force Cambridge Res. Lab., Hanscom Air Force Base, Mass.

Mullen, P. C., and S. G. Warren (1988), Theory of the optical properties of lake ice, *J. Geophys. Res.*, *93*, 8403–8414.

Neshyba, S. P., T. C. Grenfell, and S. G. Warren (2003), Representation of a nonspherical ice particle by a collection of independent spheres for scattering and absorption of radiation: 2. Hexagonal columns and plates, *J. Geophys. Res.*, *108*(D15), 4448, doi:10.1029/2002JD003302.

Painter, T. H., N. P. Molotch, M. Cassidy, M. Flanner, and K. Steffen (2007), Instruments and methods: Contact spectroscopy for determination of stratigraphy of snow optical grain size, *J. Glaciol.*, *53*, 121–127, doi:10.3189/172756507781833947.

Paterson, W. S. B. (2000), *Physics of Glaciers*, 3 ed., 481 pp., Butterworth-Heinemann, Oxford, U. K.

Pedersen, C. A., and J. G. Winther (2005), Intercomparison and validation of snow albedo parameterization schemes in climate models, *Clim. Dyn.*, *25*, 351–362, doi:10.1007/s00382-005-0037-0.

Perovich, D. K., T. C. Grenfell, B. Light, and P. V. Hobbs (2002), Seasonal evolution of the albedo of multiyear Arctic sea ice, *J. Geophys. Res.*, *107*(C10), 8044, doi:10.1029/2000JC000438.

Platnick, S., M. D. King, S. A. Ackerman, W. P. Menzel, B. A. Baum, J. C. Riedi, and R. A. Frey (2003), The MODIS cloud products: Algorithms and examples from Terra, *IEEE Trans. Geosci. Remote Sens.*, *41*, 459–473, doi:10.1109/TGRS.2002.808301.

Ranzi, R., and R. Rossi (1991), A physically based approach to modelling distributed snowmelt in a small alpine catchment, *IAHS Publ.*, *205*, 141–150.

Ricchiazzi, P., S. R. Yang, C. Gautier, and D. Sowle (1998), SBDART: A research and teaching software tool for plane-parallell radiative transfer in the Earth's atmosphere, *Bull. Am. Meteorol. Soc.*, *79*, 2101–2114, doi:10.1175/1520-0477(1998)079<2101:SARATS>2.0.CO;2.

Segal, M., J. R. Garratt, R. A. Pielke, and Z. Ye (1991), Scaling and numerical-model evaluation of snow-cover effects on the generation and modification of daytime mesoscale circulations, *J. Atmos. Sci.*, *48*, 1024–1042, doi:10.1175/1520-0469(1991)048<1024:SANMEO>2.0.CO;2.

Sergent, C., E. Pougatch, M. Sudul, and B. Bourdelles (1993), Experimental investigation of optical snow properties, *Ann. Glaciol.*, *17*, 281–287.

Sergent, C., C. Leroux, E. Pougatch, and F. Guirado (1998), Hemispherical-directional reflectance measurements of natural snow in the 0.9–1.45 $\mu$m spectral range: Comparison with adding-doubling modeling, *Ann. Glaciol.*, *26*, 59–63.

Serreze, M. C., and R. G. Barry (2005), *The Arctic Climate System*, 1st ed., *Cambridge Atmos. Space Sci. Ser.*, 385 pp., Cambridge Univ. Press, Cambridge, U. K.

Spencer, M. K., R. B. Alley, and J. J. Fitzpatrick (2006), Developing a bubble number-density paleoclimatic indicator for glacier ice, *J. Glaciol.*, *52*, 358–364, doi:10.3189/172756506781828638.

Stamnes, K., S. C. Tsay, W. Wiscombe, and K. Jayaweera (1988), Numerically stable algorithm for discrete-ordinate-method radiative transfer in multiple scattering and emitting layered media, *Appl. Opt.*, *27*, 2502–2509, doi:10.1364/AO.27.002502.

Stroeve, J., A. Nolin, and K. Steffen (1997), Comparison of AVHRR-derived and in situ surface albedo over the Greenland Ice Sheet, *Remote Sens. Environ.*, *62*, 262–276, doi:10.1016/S0034-4257(97)00107-7.

Taillandier, A.-S., F. Domine, W. R. Simpson, M. Sturm, and T. A. Douglas (2007), Rate of decrease of the specific surface area of dry snow: Isothermal and temperature gradient conditions, *J. Geophys. Res.*, *112*, F03003, doi:10.1029/2006JF000514.

van den Broeke, M., D. van As, C. Reijmer, and R. van de Wal (2004), Assessing and improving the quality of unattended radiation observations in Antarctica, *J. Atmos. Oceanic Technol.*, *21*, 1417–1431, doi:10.1175/1520-0426(2004)021<1417:AAITQO>2.0.CO;2.

Warren, S. G. (1982), Optical properties of snow, *Rev. Geophys. Space Phys.*, *20*, 67–89, doi:10.1029/RG020i001p00067.

Warren, S. G. (1984), Impurities in snow: Effects on albedo and snowmelt (review), *Ann. Glaciol.*, *5*, 177–179.

Warren, S. G., and R. E. Brandt (2008), Optical constants of ice from the ultraviolet to the microwave: A revised compilation, *J. Geophys. Res.*, *113*, D14220, doi:10.1029/2007JD009744.

Warren, S. G., and A. D. Clarke (1990), Soot in the atmosphere and snow surface of Antarctica, *J. Geophys. Res.*, *95*, 1811–1816.

Warren, S. G., and W. J. Wiscombe (1980), A model for the spectral albedo of snow. II: Snow containing atmospheric aerosols, *J. Atmos. Sci.*, *37*, 2734–2745, doi:10.1175/1520-0469(1980)037<2734:AMFTSA>2.0.CO;2.

Warren, S. G., R. E. Brandt, and P. O. Hinton (1998), Effect of surface roughness on bidirectional reflectance of Antarctic snow, *J. Geophys. Res.*, *103*, 25,789–25,807, doi:10.1029/98JE01898.

Warren, S. G., R. E. Brandt, T. C. Grenfell, and C. P. McKay (2002), Snowball Earth: Ice thickness on the tropical ocean, *J. Geophys. Res.*, *107*(C10), 3167, doi:10.1029/2001JC001123.

Winther, J. G. (1993), Short-term and long-term variability of snow albedo, *Nord. Hydrol.*, *24*, 199–212.

Wiscombe, W. J., and S. G. Warren (1980), A model for the spectral albedo of snow. I: Pure snow, *J. Atmos. Sci.*, *37*, 2712–2733, doi:10.1175/1520-0469(1980)037<2712:AMFTSA>2.0.CO;2.

Wright, A., J. Wadham, M. Siegert, A. Luckman, and J. Kohler (2005), Modelling the impact of superimposed ice on the mass balance of an Arctic glacier under scenarios of future climate change, *Ann. Glaciol.*, *42*, 277–283, doi:10.3189/172756405781813104.

Wright, A. P., J. L. Wadham, M. J. Siegert, A. Luckman, J. Kohler, and A. M. Nuttall (2007), Modeling the refreezing of meltwater as superimposed ice on a high Arctic glacier: A comparison of approaches, *J. Geophys. Res.*, *112*, F04016, doi:10.1029/2007JF000818.

Zuo, Z., and J. Oerlemans (1996), Modelling albedo and specific balance of the Greenland Ice Sheet: Calculations for the Sondre Stromfjord transect, *J. Glaciol.*, *42*, 305–317.

A. S. Gardner and M. J. Sharp, Department of Earth and Atmospheric Sciences, University of Alberta, 1-16B Earth Sciences Bldg., Edmonton, AB T6G 2E3, Canada. (alexg@ualberta.ca)